

# VL-SAFE: Vision-Language Guided Safety-Aware Reinforcement Learning with World Models for Autonomous Driving

Yansong Qu<sup>†</sup>, Zilin Huang<sup>†</sup>, Zihao Sheng<sup>†</sup>, Jiancong Chen, Sikai Chen<sup>\*</sup>, Samuel Labi

**Abstract**—Reinforcement learning (RL)-based autonomous driving policy learning faces critical limitations such as low sample efficiency and poor generalization; its reliance on online interactions and trial-and-error learning is especially unacceptable in safety-critical scenarios. Existing methods including safe RL often fail to capture the true semantic meaning of "safety" in complex driving contexts, leading to either overly conservative driving behavior or constraint violations. To address these challenges, we propose VL-SAFE, a world model-based safe RL framework with Vision-Language model (VLM)-as-safety-guidance paradigm, designed for offline safe policy learning. Specifically, we construct offline datasets containing data collected by expert agents and labeled with safety scores derived from VLMs. A world model is trained to generate imagined rollouts together with safety estimations, allowing the agent to perform safe planning without interacting with the real environment. Based on these imagined trajectories and safety evaluations, actor-critic learning is conducted under VLM-based safety guidance to optimize the driving policy more safely and efficiently. Extensive evaluations demonstrate that VL-SAFE achieves superior sample efficiency, generalization, safety, and overall performance compared to existing baselines. To the best of our knowledge, this is the first work that introduces a VLM-guided world model-based approach for safe autonomous driving. The demo video and code can be accessed at: <https://ys-qu.github.io/vlsafe-website/>

**Index Terms**—vision-language models; world model; safe reinforcement learning; autonomous driving

## I. INTRODUCTION

**A**UTONOMOUS driving technology has made tremendous strides over the past decade, transforming from a futuristic vision into an increasingly achievable reality [1], [2]. Current transportation management methods have produced significant improvements [3], [4]. Yet still, current transportation systems still struggle with inefficiencies and limited capabilities in accident prevention and traffic mobility optimization. Autonomous driving, with its advanced intelligence and automation [5], offers a promising solution. At its core, autonomous driving aims to perceive [6], understand [7], and interact [8] with complex dynamic systems in real time. Among various approaches, RL has emerged as a

promising paradigm for developing intelligent driving agents. RL-based autonomous driving systems learn control policies by interacting with the environment to maximize expected cumulative rewards.

*"A person who never made a mistake never tried anything new," said Albert Einstein.* RL's nature of trial and error (the paradigm of online RL is shown in Fig. 1 (a)) embodies this philosophy. Therefore, it is true that exploration is inevitably often accompanied by errors. Yet still, exploration in the context of autonomous driving applications could be considered unacceptable particularly in safety-critical scenarios. The more an agent interacts with the environment, the greater the potential for both progress and failure. The key lies in striking a balance between learning efficiently and avoiding harmful outcomes. To achieve this goal, several directions have been explored to enable effective exploration while maintaining safety guarantees. Offline RL removes the need for online exploration entirely by learning from pre-collected driving data, thus avoiding the safety concerns of real-time trial-and-error (Fig. 1 (b)). World models [9], [10], [11] can reduce interactions by enabling policy learning through imagined rollouts, this could significantly largely reduce risky actions and improve sample efficiency (Fig. 1 (c)). Safe RL methods explicitly incorporate cost constraints or risk-sensitive objectives into the learning process to restrict unsafe behaviors and ensure long-term safety (Fig. 1 (d)).

Though effective, each of these solutions has its drawbacks. Offline RL still fails occasionally in online testing due to the lack of safety constraints; world models can still make risky actions at the initial training stage; safe RL might learn a too conservative policy and unable to generalize due to the lack of semantic understanding of the entire context. It is intuitive to combine these methods together to complement each other's strengths and weaknesses. However, more importantly, at the core of these challenges lies a fundamental question: **how to identify risky states, semantically understand "safety", and guide policy learning accordingly?** Current methods are either prone to learn an overly conservative policy or lack a semantic understanding true meaning of "safety". As a result, they are

<sup>\*</sup> Corresponding author: Sikai Chen. <sup>†</sup> Equal contribution.

Yansong Qu is with the Lyles School of Civil and Construction Engineering, Purdue University, West Lafayette, 47907, USA (e-mail: qu120@purdue.edu).

Zilin Huang is with the Department of Civil and Environmental Engineering, University of Wisconsin-Madison, Madison, 53706, USA (e-mail: zilin.huang@wisc.edu).

Zihao Sheng is with the Department of Civil and Environmental Engineering, University of Wisconsin-Madison, Madison, 53706, USA (e-mail: zihao.sheng@wisc.edu).

Jiancong Chen is with the Lyles School of Civil and Construction Engineering, Purdue University, West Lafayette, 47907, USA (e-mail: chen5281@purdue.edu).

Sikai Chen is with the Department of Civil and Environmental Engineering, University of Wisconsin-Madison, Madison, 53706, USA (e-mail: sikai.chen@wisc.edu).

Samuel Labi is with the Lyles School of Civil and Construction Engineering, Purdue University, West Lafayette, 47907, USA (e-mail: labi@purdue.edu).

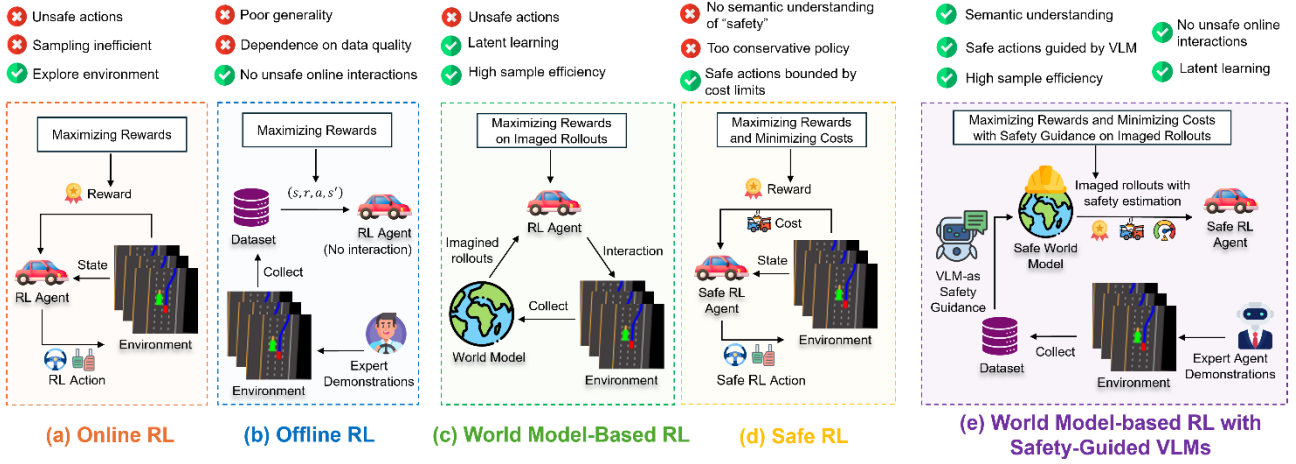


Fig. 1. Comparisons between our proposed method and related work.

unable to meaningfully differentiate between high-risk and low-risk scenarios, leading to biased-optimized policies that are biased in the sense that they either perform unsafe actions in corner cases on one hand or stay at one place all the time due to the high priority they place on safety on the other hand.

VLMs, trained on large-scale multimodal datasets, have demonstrated strong capabilities in grounding world knowledge through both visual and linguistic inputs. They have been widely applied and have demonstrated success across diverse domains [12]. Inspired by these successes, we explore the potential of using VLMs to overcome these limitations and answer the fundamental question identified in an earlier section of this paper. Conceptually, the VLM serves as a "semantic safety critic" that evaluates the risk of a given driving state based on its visual context. By providing a semantic assessment of visual scenes (e.g., "The road ahead is clear and safe to drive." and "There exist obstacles or off-road risks ahead and it is dangerous to drive."), VLMs can offer intuitive and generalizable safety signals. These signals can guide the RL agent to determine when it is appropriate to maximize rewards (e.g., travel efficiency) and when to minimize costs (e.g., avoid collisions), leading to learning of more balanced driving policy in terms of safety and mobility.

In summary, our proposed method proposes VLM-as-safety-guidance paradigm combined with world model and safe RL under offline setting to enable safety-aware policy optimization for autonomous driving (Fig. 1 (e)). The VLM's safety evaluations are served as ground truths for the world model to learn and generate safety-aware rollouts where the policy learns to perform optimal actions under safety constraints posed by safe RL. The main contributions of this work are as follows:

(1) We integrate world models and safe RL in an offline setting, where each component compensates for the limitations of the others. Offline learning avoids unsafe online exploration; the world model enhances sample efficiency through imagination; and safe RL enforces explicit safety constraints, collectively improving the safety and effectiveness of policy learning in terms of safety and mobility.

(2) We propose a novel **VLM-as-safety-guidance paradigm**, where a VLM semantically understands and

evaluates the concept of "safety" in driving scenes. This provides generalizable safety supervision that complements traditional rule-based or cost-based safety constraints posed by safe RL.

(3) We conduct comprehensive experiments in simulated driving environments, demonstrating that our method significantly improves safety, generalization, and policy robustness compared to state-of-the-art baselines.

**To the best of our knowledge, this is the first work that introduces a VLM-guided world model-based approach for safe autonomous driving.**

The remainder of this paper is organized as follows. Related work is presented in Section II. Section III describes the motivation. Section IV illustrates the preliminaries. Section V demonstrates the methodology. The experimental results are discussed in Section VI, and conclusions are summarized in Section VII.

## II. MOTIVATION

**An example from life.** We introduce our motivation starting from an intuitive life example: imagine an autonomous vehicle approaching a stopped school bus on a multi-lane road, where several children are walking across the street toward the sidewalk. The school bus has its STOP sign extended, indicating that all surrounding vehicles must come to a complete stop (Fig. 2).



Fig. 2. A real-life example to highlight the potential effectiveness of VLM-as safety guidance paradigm.

In the scenario presented in Fig. 2, a classical RL-based or offline-trained agent may continue driving or only slightly slow down, as no collision has occurred and the reward function still favors the continuance of driving in this scenario. A world model-based agent may also ignore the school bus and its STOP sign during imagined rollouts, failing to distinguish the risk

embedded in this visual context. A traditional safe RL policy may behave unpredictably, it may stop in some cases but may often fails to recognize the raised STOP sign and the presence of children, particularly if such visual cues are not explicitly encoded in the cost function or the training data. This could lead to unsafe decisions or over-generalized conservativeness, for example, treating harmless objects (such as parked vehicles or work zone cones) as equivalent threats.

In contrast, a VLM-guided policy is designed to semantically understand the scene: the raised STOP sign on the school bus and the crossing children clearly indicate a high-risk situation. Even in the absence of a collision, the VLM assigns a low safety score based on visual semantics, guiding the agent to stop proactively and yield to the pedestrians. This enables the agent to appropriately adopt caution when driving in dangerous scenarios without falling into the trap of indiscriminate conservative behavior.

This example highlights the advantage of semantic safety reasoning: it enables agents to make early, context-aware, and proportionate decisions, ultimately allowing them to act safely across a variety of road scenarios.

### III. RELATED WORK

#### A. Classical Online RL-based autonomous driving

RL offers a principled framework for sequential decision-making and has gained significant traction in autonomous systems research [13]. Despite its promise, RL faces several limitations in practical deployment. Generalization remains a key challenge, agents trained in simulation often fail in other unseen environments [14]. Additionally, standard RL algorithms do not explicitly consider safety, potentially leading to risky or catastrophic behavior during both training and execution. By leveraging world model and VLM-based safety guidance under offline setting, our proposed method can largely overcome these shortcomings.

#### B. Offline RL

By decoupling learning from real-time interactions, offline RL enables the use of previously collected expert demonstrations to develop safety-oriented policies [15]. Previous researchers [16] have proposed a novel offline RL method that learns a conservative (safe) policy using latent safety constraints and optimizes cumulative rewards under these constraints via advantage-weighted learning in the latent space. However, RL policies trained on limited or suboptimal datasets often suffer from distributional shift, making them prone to selecting out-of-distribution actions [17], [18]. Furthermore, safety signals (e.g., risk annotations, constraint violations) are often sparse or unavailable in the offline dataset [19]. Moreover, offline RL suffers from limited generalization due to fixed data, our method leverages a world model to generate imagined rollouts, thereby enhancing data diversity and sample efficiency.

#### C. World model

World models learn to simulate environment dynamics from data, enabling agents to plan or imagine rollouts internally [9], [10], [11]. They help decouple policy learning from direct environment interaction by simulating future trajectories, thus

improve sample efficiency, particularly in safety-critical or data-scarce domains such as autonomous driving [20], [21], [22]. However, a limitation of standard world models is that they may produce inaccurate or unrealistic rollouts, particularly during the early stages of training. This can lead to unsafe actions, as the policy is optimized based on flawed imagined trajectories. To mitigate this issue, we propose a safety-aware world model that performs semantic safety evaluation on each imagined state. By identifying and guiding the policy away from risky trajectories, this mechanism enables safer policy learning.

#### D. Safe RL

Safe RL aims to optimize agent behavior while satisfying safety constraints throughout training and deployment. Constrained optimization approaches solve the problem by incorporating Lagrangian multipliers or dual gradient methods [23]. Risk-sensitive approaches formulate objectives that consider conditional value-at-risk, worst-case return, or variance-based measures [24]. Other lines of work leverage control-theoretic techniques [25] or Lyapunov-based constraints [26], to ensure safety in continuous control systems. These methods are effective but lack semantic understanding of safety and often overlook driving context, leading to biased (overly aggressive or overly conservative) policies. In contrast, we leverage a VLM to derive safety scores based on scene semantics, enabling more context-aware and balanced safe policy learning.

#### E. VLMs in autonomous driving

VLMs jointly process visual inputs and natural language, has been shown to achieve success in general-purpose AI tasks such as image captioning [27], [28], answering visual questions [29], [30], and embodied intelligence [31]. Also, VLMs are appealing in autonomous driving domains, where they can provide semantic understanding of driving scenes [32], language-guided planning [33], curriculum learning [34], and decision-making [35]. However, their application in the safety domain of autonomous driving remains relatively underexplored. Similar works are discussed herein: LORD [36] uses undesired language goals to shape rewards and offers limited guidance by focusing only on states to avoid. To improve on this, VLM-RL [35] proposed a contrastive language goal by contrasting both desired and undesired goals combined with vehicle state information for richer reward signals. However, none of them have fully explored the usage of VLMs in safe RL theoretically under autonomous driving domains. The present paper addresses this gap.

### IV. PRELIMINARIES

#### A. Markov Decision Processes

A Markov Decision Process (MDP) is defined as a tuple  $M = (\mathcal{S}, \mathcal{A}, \mathcal{T}, \mathcal{R}, \mu, \gamma)$ , where  $\mathcal{S}$  denotes state space,  $\mathcal{A}$  denotes action space,  $\mathcal{T}: \mathcal{S} \times \mathcal{A} \times \mathcal{S} \rightarrow [0,1]$  denotes the transition probability function,  $\mathcal{R}: \mathcal{S} \times \mathcal{A} \rightarrow \mathbb{R}$  denotes reward function,  $\mu(\cdot): \mathcal{S} \rightarrow [0,1]$  denotes the initial state distribution, and  $\gamma \in [0,1]$  denotes the discount factor. At each timestep, the agent observes state  $s \in \mathcal{S}$ , and agent selects an action  $a \in \mathcal{A}$ . The environment transitions to the next state  $s'$  via

transition  $\mathcal{T}(s'|s, a)$ . The agent then receives the immediate reward  $R(s, a)$ . Also, some algorithms demand continuous tuples as inputs which can be formed as a trajectory  $\tau = (s_0, a_0, r_0, s_1, a_1, r_1, \dots)$ , its return is formulated as the discounted sum of rewards:  $g(\tau; R) = \sum_{t=0}^T \gamma^t R(s_t, a_t)$ . The agent's goal is to learn a policy  $\pi(a|s)$  that maximizes the expected return  $G(\pi) = \mathbb{E}_\pi[g(\tau(\pi); R)]$ . In practice, the policy will maximize state value function  $V(s) = \mathbb{E}_{\tau \sim \pi_\psi}[\sum_{t=0}^T \gamma^t R(s_t, a_t)]$  or action-state value function  $Q(s, a) = \mathbb{E}_{\tau \sim \pi_\psi}[\sum_{t=0}^T \gamma^t R(s_t, a_t)]$ .

### B. Offline RL

In contrast to online RL methods, offline RL uses a fixed dataset to learn an optimal policy without further interacting with online environment. Also, unlike Imitation Learning (IL), offline RL does not mimic expert behavior directly, thus can infer better actions than those in datasets and continuously improve. Offline RL is effective; however, its generalization is limited by the fixed dataset. In contrast, our proposed method incorporates a world model to generate imagined rollouts, thereby expanding the data distribution and improving sample efficiency. Offline RL usually uses approximate dynamic programming to minimize temporal difference (TD) error:

$$L_{TD}(\theta) = \mathbb{E}_{(s,a,s') \sim \mathcal{D}} \left[ \left( r(s, a) + \gamma \max_a Q_\theta(s', a') - Q_\theta(s, a) \right)^2 \right] \quad (1)$$

where  $\mathcal{D}$  denotes the offline dataset,  $Q_\theta(s, a)$  denotes the Q-function parameterized by  $\theta$ ,  $Q_\theta(s, a)$  denotes the target network with soft parameters updates. A major limitation of Offline RL is Q-value overestimation, primarily resulting from extrapolation errors when evaluating actions that are not well-supported by the dataset.

### C. World model-based safe RL

Safe RL is formulated as a constrained MDP  $\mathcal{M} = (\mathcal{S}, \mathcal{A}, \mathcal{T}, \mathcal{R}, \mathcal{C}, \mu, \gamma)$ , where  $\mathcal{C}$  is a cost function set containing

cost functions  $\mathbf{c}: \mathcal{S} \times \mathcal{A} \rightarrow [0, C_{\max}]$ . Given a policy  $\pi_\psi$ , the reward function and cost function of safe RL can be defined as:

$$J^R(\pi_\psi) = \mathbb{E}_{a_t \sim \pi_\psi, s_{t+1} \sim p_{\theta, s_0 \sim \mu}} \left[ \sum_{t=0}^T r_t \mid s_0 \right] \quad (2)$$

$$J_i^C(\pi_\psi) = \mathbb{E}_{a_t \sim \pi_\psi, s_{t+1} \sim p_{\theta, s_0 \sim \mu}} \left[ \sum_{t=0}^T c_t^i \mid s_0 \right] \leq d^i, \forall i \in \{1, \dots, C\} \quad (3)$$

where  $c_t^i$  is the  $i$ -th safety constraint that the  $\pi_\psi$  that learn to obey, and  $d^i$  is the cost threshold according to  $c_t^i$ . The safe RL thus can be defined as:

$$\max_{\psi} J^R(\pi_\psi) \text{ s.t. } J_i^C(\pi_\psi) \leq d^i, \forall i \in \{1, \dots, C\} \quad (4)$$

When we define the safe RL under model-based setting, we use the generated rollouts by  $\mathcal{T}$ , for example, a world model, to train the policy using predicted costs and rewards. Also, by introducing a Lagrange method, the safe RL problem can be reformulated into a min-max form:

$$\max_{\lambda \geq 0} \max_{\psi} [J^R(\pi_\psi) - \sum_{i=1}^C \lambda_i (J_i^C(\pi_\psi) - d^i)] \quad (5)$$

where inner maximization optimizes the original reward objective while penalizing violations of the constraints through the Lagrange multipliers  $\lambda_i$ ; the outer minimization finds the best set of multipliers  $\lambda_i$  to enforce the constraints by adjusting penalties. However, safe RL only constraints the cost under a threshold, not considering the entire driving context. Instead, our proposed VLM-as-safety-guidance paradigm is designed to be capable of semantically understanding the driving context and infer safety scores for each state.

### D. VLMs

VLMs are a class of deep neural networks that integrate visual and textual modalities, enabling joint understanding of images and text. Among them, a notable class of VLMs is CLIP [37]. CLIP projects the multi-modal inputs into latent space to

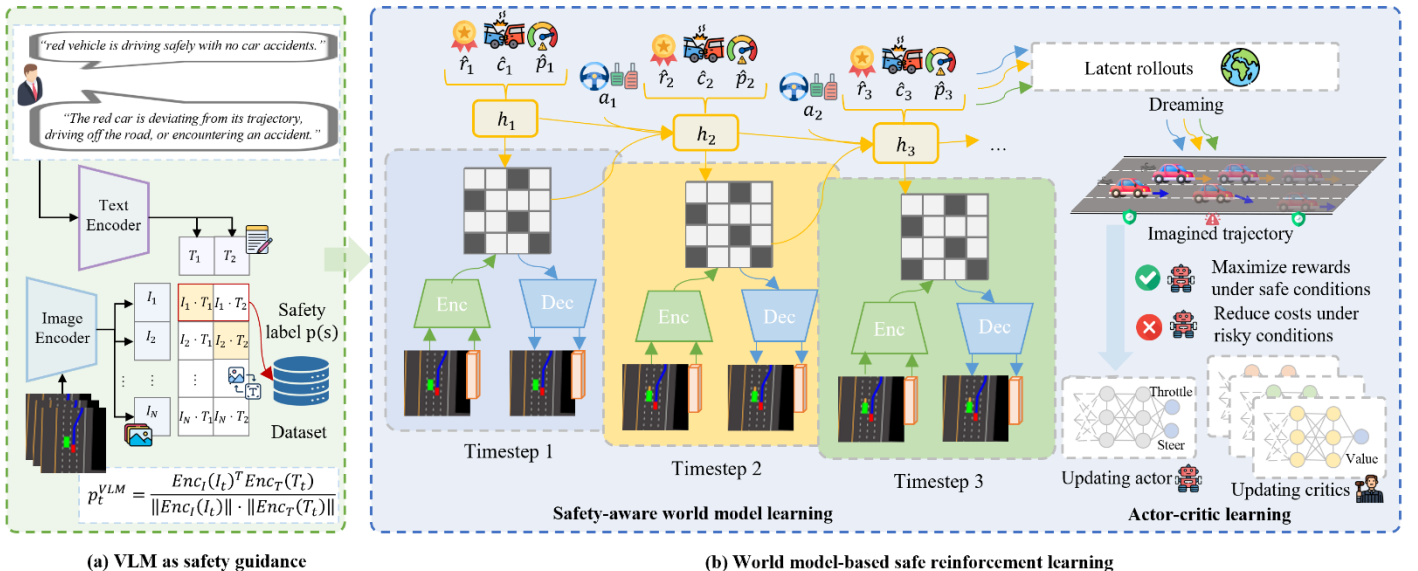


Fig. 3. Overall framework of VL-SAFE.

calculate cosine similarity between two modalities. In our work, we primarily use the pretrained CLIPs without further fine-tuning.

#### D. Problem Statement

We model the task of training an agent as a constrained MDP, similar to [38]. The agent’s object is to learn an optimal safe policy  $\pi_\psi: \mathcal{S} \rightarrow \mathcal{A}$  that maximizes the expected cumulative reward while reduces the violations of safety constraints. A key challenge is how to evaluate the risk of current state  $s$ . Our intuition is to leverage the semantic understanding ability of pretrained CLIPs to estimate the probability of safety for each state. The probabilities of safety will be used by world model as ground truths to predict the safety of future rollouts which are then used for training policy. Under this setting, we can reformulate the constrained MDP as  $\mathcal{M} = (\mathcal{S}, \mathcal{A}, \mathcal{T}, \mathcal{R}, \mathcal{C}, \mathcal{P}, \mu, \gamma)$ , where  $p \in \mathcal{P}$  denotes the safety probability of each state and is calculated by CLIPs.

### V. METHODOLOGY

As shown in Fig.3, the proposed method VL-SAFE has two phases: the first phase generates ground-truth safety estimations using CLIPs [37] for each state in offline dataset collected by expert agent (Section V-A); and the second stage learns a safety-aware world model to generate imagined rollouts along with predicted safety estimations for actor-critic learning (Section V-B). The pseudo-code of VL-SAFE is presented in Appendix A.

#### A. VLM as safety guidance

We propose using VLM-as-safety-guidance paradigm based on the premise that **the estimation of safety can be considered instantaneously when the estimation function can truly understand the real meaning of “safety”**. Our paradigm not only shares a similar goal with reachability estimation function (REF) [39] but also offers a key advantage: it can assess each state directly by measuring the similarity between visual observations and natural language safety descriptions. This enables a softer, semantic-aware estimation of the extent to which a situation is safe or unsafe.

**Definition 1 (VLM-as-Safety-Guidance Paradigm).** *Given the vision encoder  $Enc_I$ , language encoder  $Enc_L$ , image input  $I_t$  and text prompt  $T_t$  (e.g., “the ego vehicle is driving safely with no car accidents”), the encoders map image and text inputs into the same hidden space and measure the similarity between the image and text embeddings:*

$$p_t^{VLM} = \text{Sim}(Enc_I(I_t), Enc_L(T_t)) \quad (6)$$

*Previous works [35], [36] adopt CLIP [37] as the pretrained VLM and cosine similarity as the  $\text{Sim}(\cdot, \cdot)$  indicator. We also follow this diagram.*

$$p_t^{VLM} = \frac{Enc_I(I_t)^T Enc_L(T_t)}{\|Enc_I(I_t)\| \cdot \|Enc_L(T_t)\|} \quad (7)$$

*However, a key difference is that our proposed model does not use the  $p_t^{VLM}$  as the direct safety estimation directly, instead, given a sequence of data  $\mathcal{B} = (x_{1:T}, a_{1:T}, r_{1:T}, c_{1:T})$ , our model generates  $p_{1:T}^{VLM}$  as ground truth by CLIP, and then uses function  $p(s)$  to approximate to  $p_{1:T}^{VLM}$  in world model. This can*

*significantly reduce the inference time costed by CLIP and save computation resources.*

As shown in Fig. 3 (a), the VLM acts as a judge here: it derives safety scores for each state in offline dataset. The safety scores serve as ground-truth data for predicting safety estimations in imagined rollouts in the world model, which will be discussed in later section. We also demonstrate the analysis of stability of VLM-as safety guidance in Appendix B. 1.

#### B. World model-based safe RL

As shown in Fig. 3 (b), we first train a safety-aware world model which predicts not only rewards and costs but also safety estimations for each state in the imagined rollouts. Without such safety guidance, the RL agent must rely on extensive trial-and-error training to gradually infer which states are safe and which are unsafe, often resulting in slow convergence and unsafe actions during early learning. In contrast, our VLM-as-safety-guidance paradigm provides explicit semantic signals that directly inform the policy which states are safe and should be used to maximize rewards, and which states are unsafe and should be used to minimize costs. This targeted guidance allows the agent to efficiently learn a safe and balanced policy with significantly reduced exploration overhead.

**Safety-aware World Model Learning.** We consider this section as  $\mathcal{M} = (\mathcal{S}, \mathcal{A}, \mathcal{T}, \mathcal{R}, \mathcal{C}, \mathcal{P}, \mu, \gamma)$  under offline safe RL setting with world model “dreaming” the future rollouts along with safety estimations for policy training. Given a sequence of data  $\mathcal{B} = (x_{1:T}, a_{1:T}, r_{1:T}, c_{1:T}, p_{1:T})$  sampled from the offline dataset, we use an adopted DreamerV3 [9] as the world model to generate rollouts with explicit safety indicators:

$$\begin{aligned} \text{Observation encoder:} & \quad z_{1:T}^0 \sim q_\theta(z \mid h_{1:T}, x_{1:T}) \\ \text{Dynamics predictor:} & \quad \hat{z}_{1:T}^l \sim p_\theta(z \mid h_{1:T}^l) \\ \text{Sequence model:} & \quad h_{1:T}^{l+1} = f_\theta(h_{1:T}^l, z_{1:T}^l, a_{1:T}) \\ \text{Actor:} & \quad \hat{a}_{1:T}^l \sim \pi_\psi(a \mid z_{1:T}^l) \\ \text{Decoder:} & \quad \hat{x}_{1:T}^l \sim p_\theta(x \mid h_{1:T}^l, z_{1:T}^l) \\ \text{Reward predictor:} & \quad \hat{r}_{1:T}^l \sim p_\theta(r \mid h_{1:T}^l, z_{1:T}^l) \\ \text{Cost predictor:} & \quad \hat{c}_{1:T}^l \sim p_\theta(c \mid h_{1:T}^l, z_{1:T}^l) \\ \text{Continue predictor:} & \quad \hat{b}_{1:T}^l \sim p_\theta(b \mid h_{1:T}^l, z_{1:T}^l) \\ \text{Safety predictor:} & \quad \hat{p}_{1:T}^l \sim p_\theta(p \mid h_{1:T}^l, z_{1:T}^l) \end{aligned} \quad (8)$$

where  $l$  represents the horizon of the generated rollouts. The world model receives a trajectory of observations  $x_{1:T}$ , for example, the agent’s Bird’s-Eye View (BEV) images, the observations  $x_{1:T}$  are encoded into initial hidden presentations  $z_{1:T}^0 \sim q_\theta(z_{1:T} \mid h_{1:T}, x_{1:T})$ , which are used to generate rollouts. Then the current recurrent states  $h_{1:T}^{l+1} = f_\theta(h_{1:T}^l, z_{1:T}^l, a_{1:T})$  are generated by the sequence model using recurrent states  $h_{1:T}^l$ , hidden presentation  $z_{1:T}^l$  and action  $a_{1:T}$ . We seek to conduct a multi-step prediction at the each timestep. Therefore, we use a dynamics predictor to predict the hidden presentation  $\hat{z}_{1:T}^l$  based on solely on  $h_{1:T}^l$ . We also use reward predictor, continue predictor, cost predictor and safety predictor to predict the reward, continuity, cost, and safety probability, respectively. Finally, the decoder re-constructs the original observation to ensure that  $\{h_{1:T}, z_{1:T}\}$  have condensed all necessary information.

The following loss functions are used to train the world model:

$$\begin{aligned} \mathcal{L}_{\text{pred}}(\theta) = & -\ln p_\theta(x \mid h_{1:T}^l, z_{1:T}^l) \\ & -\ln p_\theta(r \mid h_{1:T}^l, z_{1:T}^l) \\ & -\ln p_\phi(c \mid h_{1:T}^l, z_{1:T}^l) \\ & -\ln p_\phi(p \mid h_{1:T}^l, z_{1:T}^l) \end{aligned} \quad (9)$$

$$\mathcal{L}_{\text{dyn}}(\theta) = \max(1, \text{KL}[\text{sg}(q_\theta(z \mid h_{1:T}, x_{1:T})) \parallel p_\theta(z \mid h_{1:T}^l)]) \quad (10)$$

$$\mathcal{L}_{\text{rep}}(\theta) = \max(1, \text{KL}[sg(p_\theta(z \mid h_{1:T}^l)) \parallel q_\theta(z \mid h_{1:T}, x_{1:T})]) \quad (11)$$

The losses are scaled and summed for calculating gradients:

$$\mathcal{L}(\theta) \doteq \mathbb{E}_{q_\theta} \sum_{t=1}^T (\beta_{\text{pred}} \mathcal{L}_{\text{pred}}^t(\theta) + \beta_{\text{dyn}} \mathcal{L}_{\text{dyn}}^t(\theta) + \beta_{\text{rep}} \mathcal{L}_{\text{rep}}^t(\theta)) \quad (12)$$

where  $\beta_{\text{pred}}$ ,  $\beta_{\text{dyn}}$ , and  $\beta_{\text{rep}}$  are hyper-parameters to balance different loss terms.

**Actor-critics Learning.** We use the generated rollouts to train actor-critic networks. Motivated by [38], we use a separate value network  $V_\phi(s) = \mathbb{E}_{a \sim \pi_\psi(\cdot \mid s)}[Q_\phi(s, a)]$  only conditioned on states to mitigate the over-estimation problem. The value network is optimized by expectile regression:

$$\begin{aligned} \mathcal{L}_V(\phi) = & \mathbb{E}_{\tau \sim \mathcal{D}, \pi_\psi, p_\theta} \left[ \left| \kappa \right. \right. \\ & \left. \left. - \mathbb{1}\{Q_\phi(\hat{s}_t^j, \hat{a}_t^j) - V_\phi(\hat{s}_t^j) \right. \right. \\ & \left. \left. < 0\} \mid (Q_\phi(\hat{s}_t^j, \hat{a}_t^j) - V_\phi(\hat{s}_t^j))^2 \right] \end{aligned} \quad (13)$$

Also, during the early stages of offline training, the world model may not be able to generate accurate rewards. The real rewards from the offline dataset can better guide the critic's learning process. The critic loss [38] is:

$$\mathcal{L}_Q(\phi) = \mathcal{L}_Q^1(\phi) + \mathcal{L}_Q^2(\phi) \quad (14)$$

where  $\mathcal{L}_Q^1(\phi) = -\frac{1}{LT} \mathbb{E}_{\tau \sim \mathcal{D}, \pi_\psi, p_\theta} \left[ \sum_{t=1}^T \sum_{l=1}^L (Q_\phi(\hat{s}_t^l, \hat{a}_t^l) - R_t^l)^2 \right]$ ,  $\mathcal{L}_Q^2(\phi) = -\frac{1}{T} \mathbb{E}_{\tau \sim \mathcal{D}, \pi_\psi, p_\theta} \left[ \sum_{t=1}^T \left[ Q_\phi(\hat{s}_t^0, \mathbf{a}_t) - (\mathbf{r}_t + \gamma V_\phi(\mathbf{s}_{t+1}^0)) \right]^2 \right]$ ,  $L$  denotes the horizon,  $R_t^l = V_\phi(\hat{s}_t^l)$ , and  $R_t^l = \hat{\mathbf{r}}_t^l + \gamma((1-\lambda)V_\phi(\hat{s}_t^l) + \lambda R_{t+1}^l)$ . The second term acts as a regularization term to improve learning efficiency.

For safe policy learning, the key point is to keep a balance between maximizing rewards and minimizing costs. An intuition behind this is to prioritize reward maximization under safe conditions and sideline it under dangerous conditions. However, how to quantify the safety for each state is challenging. We assume  $p(s)$  measures the safety of the state  $s$  and  $1 - p(s)$  measures the risk. Inspired by [38], the problem can be formulated as:

$$\begin{aligned} \max_{\pi_\psi} \mathbb{E}_s \left[ \left( A^r(\mathbf{s}, \mathbf{a}) - \Phi(V_\phi^c(\mathbf{s}), \lambda_p^k, \mu^k) \right) \cdot p(s) \right. \\ \left. - A^c(\mathbf{s}, \mathbf{a}) \cdot (1 - p(s)) \right] \end{aligned} \quad (15)$$

Eq. (15) is subject to  $D_{\text{KL}}(\pi_\psi \parallel \pi_b) \leq \epsilon$ , and

$$\begin{aligned} & \Phi(V_\phi^c, \lambda_p^k, \mu^k) \\ = & \begin{cases} \lambda_p^k V_\phi^c + \frac{\mu^k}{4} (V_\phi^c)^2 & \text{if } \lambda_p^k + \frac{\mu^k}{2} V_\phi^c \geq 0 \\ -\frac{(\lambda_p^k)^2}{\mu^k} & \text{otherwise} \end{cases} \end{aligned} \quad (16)$$

where  $\lambda_p^k$  and  $\mu^k$  are Lagrange multipliers,  $A^r(\mathbf{s}, \mathbf{a}) = Q_\phi^r(\mathbf{s}, \mathbf{a}) - V_\phi^r(\mathbf{s})$  and  $A^c(\mathbf{s}, \mathbf{a}) = Q_\phi^c(\mathbf{s}, \mathbf{a}) - V_\phi^c(\mathbf{s})$  are advantage functions, and the optimal policy (See Appendix B. 2 for more details):

$$\pi^*(\mathbf{a} \mid \mathbf{s}) = \frac{1}{Z} w \cdot \pi_b(\mathbf{a} \mid \mathbf{s}) \quad (17)$$

$$\begin{aligned} w = & p(s) \cdot \exp(\beta_1 A^r(\mathbf{s}, \mathbf{a})) + (1 - p(s)) \\ & \cdot \exp(-\beta_2 A^c(\mathbf{s}, \mathbf{a})) \end{aligned} \quad (18)$$

Intuitively, the weight  $w$  decides the proportion of policy updates according to the advantage of rewards and updates according to the advantage of costs; and  $u_\psi^\pi$  measures the safety of the trajectory. By adopting the  $p(s_t)$  as the safety indication, we have the final policy loss as follows:

$$\begin{aligned} \mathcal{L}_\pi(\psi) = & -\mathbb{E}_{\tau \sim \mathcal{D}} \left[ \sum_{t=1}^T (w \cdot \log \pi_\psi(\mathbf{a}_t \mid \mathbf{s}_t) \right. \\ & \left. + \eta E[\pi_\psi(\mathbf{a}_t \mid \mathbf{s}_t)]) \right. \\ & \left. - \Phi(V_\phi^c(\mathbf{s}_t), \lambda_p^k, \mu^k) \cdot p(s) \right] \end{aligned} \quad (19)$$

### C. Analysis

#### Connection to Advantage-Weighted Methods (AWMs).

To better understand how VLM-as-safety-guidance functions within our framework, we draw connections to AWMs, using weighted behavior cloning (WBC) as a representative example. WBC, an extension of behavioral cloning (BC), assigns importance weights to different expert samples based on their advantage. The WBC objective [40] is as follows:

$$\mathcal{L}_{\text{WBC}}(\theta) = \frac{1}{\sum_{i=1}^N w_i} \sum_{i=1}^N w_i \cdot \ell(\pi_\theta(a_i \mid s_i), a_i) \quad (20)$$

In our approach, we similarly assign weights to each state-action pair in the imagined rollouts, as shown in Eq. (18). The weight term combines both reward and cost advantages, and is modulated by a VLM-derived safety probability, which dynamically balances the influence of reward-seeking and cost-avoidance. The intuition is that the agent should prioritize reward maximization in safe conditions, and focus on cost minimization when encountering potentially risky situations, where the timing and degree of this tradeoff is guided by the semantic understanding provided by the VLM.

## VI. EXPERIMENTS

### A. Experiment Setting

**Simulation platform.** We use CarDreameer [41], an autonomous driving platform based on CARLA simulator [42], as our simulation platform with default settings. It offers multiple challenging driving tasks. We mainly adopt four tasks for evaluation, including four lanes, left turn, navigation, right turn.

**Observation space.** We use the BEV image with planning trajectory and intention sharing of background vehicles painted as inputs, the shape of BEV is (64, 64, 3).

**Action space.** The action space has a shape of (15,) and is composed of all combinations of discrete acceleration and steering values. Specifically, it is formed by the Cartesian product of discrete acceleration = [-2.0, 0.0, 2.0] (discrete values of acceleration) and discrete steering = [-0.6, -0.2, 0.0, 0.2, 0.6] (discrete values of steering angles), resulting in  $3 \times 5 = 15$  discrete action pairs.

**Data collection.** Our RL framework is mainly trained on offline setting. Therefore, we also need to collect data for the training process. For CarDreamer, we collect data with well-trained Dreamerv3 [9] agents.

**Network structure.** We use MLP to process vector inputs and CNN to process images. When world model is used, the policy is trained on latent representations instead of raw inputs, we use the same structure as [9].

**Driving scenarios.** All tasks in the CarDreamer simulation platform are conducted on Town 03 and Town 04 maps under CARLA which provides realistic urban and suburban layouts with diverse traffic elements. As shown in Fig. 4, the scenarios cover various road geometries and traffic situations essential for testing generalization and robustness in the context of autonomous driving policies.

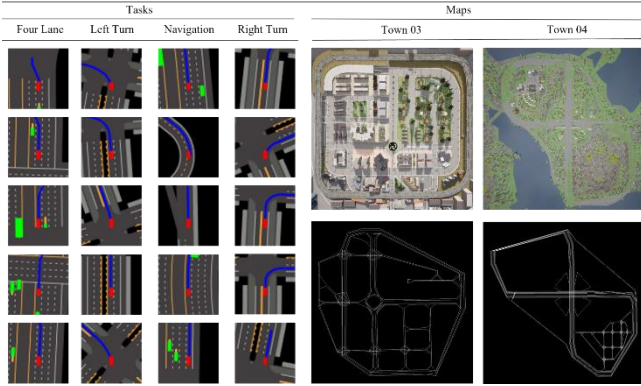


Fig. 4. Driving scenarios and maps.

## B. Evaluation metrics

**Return** represents the summed rewards in one episode. **Cost** represents the summed costs in one episode. **Average speed (AS)** represents the average speed on the x-y plane in one episode. **Waypoint completion (WC)** represents the number successfully arrived waypoints in one episode. Similar to WC, **travel distance (TD)** represents distance that the agent travels in one episode. **Arrive rate (AR)** represents the rate of successfully complete routes among the latest 10 episodes. **Collision rate (CR)** represents the rate of collisions among the latest 10 episodes. Inspired by [35], we also use **time-based collision frequency (TCF)** and **distance-based collision frequency (DCF)** to measure collisions per 1000 time steps and collisions per kilometer traveled, respectively. **Collision speed (CS)** represents the average collision speed among the latest 10 episodes.

## D. Comparison experiments

We compare our proposed method with a comprehensive set of state-of-the-art baselines in Table I, covering online RL, offline RL, and world model-based (safe) RL approaches. The online methods include Proximal Policy Optimization (PPO) [43], Soft Actor-Critic (SAC) [44], and Deep Q-Network (DQN) [45]. The offline baselines consist of Behavior Cloning (BC), Conservative Q-Learning (CQL) [18], and Implicit Q-Learning (IQL) [17]. For world model-based (safe) RL, we include Dreamerv3 [9] and FSOP [38]. Unless otherwise specified, all baselines follow the default settings provided by their respective implementations, as detailed in Appendix C. Green highlights indicate the best performance, while light green denotes the second-best performance.

In terms of the core optimization objectives, Return and Cost, VL-SAFE achieves the best results in three out of four tasks (Left Turn, Navigation, and Right Turn). Although DQN performs best in the Four Lane scenario, it is trained online for 1M timesteps, while VL-SAFE is trained with only 350k, demonstrating the efficiency of our method.

Regarding the mobility metrics (AS, WC, and TD), Dreamerv3 and FSOP generally show better performance, as they favor more aggressive and exploratory behavior. VL-SAFE, on the other hand, is designed to be safety-conscious and conservative, which leads to slightly lower mobility but aligns with its core objective of safer policy learning.

In terms of safety metrics (AR, CR, TCF, DCF, and CS), SAC and IQL may seem to perform best. However, considering their poor mobility performance (e.g., low AS and WC), these models often remain nearly stationary (very slow average speed), indicating failure to learn effective driving policies. In contrast, VL-SAFE strikes a superior balance between safety and mobility, making it the most effective and risk-aware solution overall.

## E. Ablation experiments

To evaluate the contributions of different components in our framework, we conduct an ablation analysis with three variants: VL-SAFE-NCNL, VL-SAFE-NC, and VL-SAFE. VL-SAFE-NCNL (No CLIP, No Lagrangian) refers to our proposed method without the CLIP-based safety guidance and without the Lagrangian-based cost constraints, relying only on conventional reward learning; its framework is same to Dreamerv3 [9]. VL-SAFE-NC (No CLIP) disables only the CLIP-based safety guidance while retaining the Lagrangian-based cost constraints to regulate risky behaviors; it adopts the reachability estimation as FSOP [38] did. Finally, VL-SAFE represents the full version of our proposed method, integrating both CLIP-based safety guidance and Lagrangian-based cost constraints to achieve safer and more efficient driving behavior. We evaluate these variants on the CarDreamer simulation platform across four tasks: Four Lane, Left Turn, Navigation, and Right Turn. The experimental results are summarized in Table II.

Overall, VL-SAFE consistently outperforms the other variants across all tasks. For example, in terms of the Return metric, VL-SAFE achieves 552.43 in the Four Lane task and 1074.96 in the Navigation task, both significantly higher than VL-SAFE-NCNL (326.95 and 528.86, respectively) and VL-SAFE-NC (429.18 and 775.17, respectively). This

TABLE I  
COMPARISON OF BASELINES AND VL-SAFE UNDER CARDREAMER

Four Lane										
Models	Return ↑	Cost ↓	AS ↑	WC ↑	TD ↑	AR ↑	CR ↓	TCF ↓	DCF ↓	CS ↓
PPO	356.48	79.32	2.15	71.5	75.64	0.24	0.09	0.2	1.1	3.04
SAC	96.73	28.35	0.36	20.18	17.9	0	0	0	0	0
DQN	612.33	57.79	4.69	151.54	149.96	0.81	0.11	0.33	0.73	4.25
BC	-85.39	156.46	8.76	112.35	137.13	0.59	0.2	1.29	1.48	9.51
CQL	110.42	101	5.81	104.15	120.55	0.54	0.13	0.45	1.1	7
IQL	-43.38	67.35	0.08	2.55	3.41	0	0.01	0.01	0	1.22
DreamerV3	326.95	71.81	6.3	135.6	149.49	0.67	0.2	0.89	1.46	8.37
FSOP	429.18	73.15	5.6	137.7	144.58	0.52	0.15	0.25	0.92	5.6
VL-SAFE	552.43	69.17	4.25	146.7	132.55	0.7	0.05	0.34	0.46	5.22
Left Turn										
Models	Return ↑	Cost ↓	AS ↑	WC ↑	TD ↑	AR ↑	CR ↓	TCF ↓	DCF ↓	CS ↓
PPO	208.75	35.59	1.63	37.94	34.83	0	0	0	0	0
SAC	110.2	0.28	0.31	18.86	15.5	0	0	0	0	0
DQN	214.11	44.18	3.23	45.88	61.17	0.9	0	0	0	0
BC	112.56	8.04	6.88	57.01	61.67	0.97	0	0	0	0
CQL	129.96	3.53	4.48	47.88	47.02	0.67	0	0	0	0
IQL	-1.47	0	0	0	0	0	0	0	0	0
DreamerV3	305.42	17.63	4.14	63	61.54	1	0	0	0	0
FSOP	281.87	0.22	5.12	70.9	61	1	0	0	0	0
VL-SAFE	358.7	1.68	2.18	71.5	60.63	0.94	0	0	0	0
Navigation										
Models	Return ↑	Cost ↓	AS ↑	WC ↑	TD ↑	AR ↑	CR ↓	TCF ↓	DCF ↓	CS ↓
PPO	434.51	68.5	1.62	82.95	70.13	0	0.02	0.04	0.14	0.18
SAC	-11.03	12.38	0	0.13	0.14	0	0	0	0	0
DQN	344.74	40.93	4.47	163.59	156.4	0	0.07	0.16	0.41	0.97
BC	-90.54	124.89	8.84	262.16	302.86	0	0.16	0.46	0.68	5.27
CQL	231.76	110.19	6.01	235.41	239.74	0	0.13	0.29	0.57	5.12
IQL	-177.51	217.15	0.25	3.54	5.36	0	0.02	0.03	3.67	0.03
DreamerV3	528.86	48.41	7.08	297.55	321.43	0	0.1	0.39	0.36	3.04
FSOP	775.17	54.4	6.73	359	305.04	0	0.08	0.37	0.61	3.96
VL-SAFE	935.63	0.55	3.57	246.6	178.62	0	0.01	0.04	0	0
Right Turn										
Models	Return ↑	Cost ↓	AS ↑	WC ↑	TD ↑	AR ↑	CR ↓	TCF ↓	DCF ↓	CS ↓
PPO	288.4	10.59	1.96	52.58	42.36	0.65	0	0	0	0
SAC	-8.32	96.57	0.31	14.51	13.97	0	0	0	0	0
DQN	46.04	36.46	0.49	10.96	15.11	0.14	0	0	0	0
BC	107.67	7.76	6.28	47.62	45.26	0.83	0	0	0	0
CQL	67.12	77.04	4.91	44.12	45.35	0.77	0	0	0	0
IQL	-3.88	31.43	0.14	3.78	4.11	0	0	0	0	0
DreamerV3	318.44	2.67	3.5	59.5	48.37	0.85	0	0	0	0
FSOP	258.61	0.72	4.49	60.9	48.01	0.93	0	0	0	0
VL-SAFE	315.17	0	2.53	58.1	43.5	0.89	0	0	0	0

demonstrates the effectiveness of integrating both CLIP-based safety guidance and Lagrangian-based cost constraints.

In terms of safety, VL-SAFE also achieves the best performance. Specifically, it consistently obtains the lowest Cost across all four tasks, with values of 69.17, 0.21, 9.15, and 0.0, respectively, highlighting its superior ability to minimize risky behaviors during driving.

We further analyze how this safety is achieved. Considering the AS metric, VL-SAFE's average speed is slightly lower than the other variants across all tasks, while its CS is also the smallest. We infer that VL-SAFE achieves more precise speed control, enabling it to better follow target trajectories. This is further reflected in the higher Return-to-Cost ratio per meter

traveled, indicating that VL-SAFE maintains a fine balance between performance and caution at every step.

Regarding safety-related metrics, including CR, TCF, and DCF, VL-SAFE consistently achieves the best performance, validating the effectiveness of the proposed VLM-based safety guidance for reinforcement learning-based autonomous driving.

Moreover, we observe that VL-SAFE-NCNL exhibits significantly higher Cost than the other variants in all tasks except Four Lane, emphasizing the importance of Lagrangian-based cost constraints for reducing unsafe behaviors. However, simply applying Lagrangian methods, as in VL-SAFE-NC, may lead to performance degradation in some tasks (e.g., Left Turn and Right Turn). This suggests that Lagrangian methods alone

TABLE II  
ABLATION RESULTS

Four Lane										
Variants	Return ↑	Cost ↓	AS ↑	WC ↑	TD ↑	AR ↑	CR ↓	TCF ↓	DCF ↓	CS ↓
VL-SAFE-NCNL	326.95	71.81	6.3	135.6	149.49	0.67	0.2	0.89	1.46	8.37
VL-SAFE-NC	429.18	73.15	5.6	137.7	144.58	0.52	0.15	0.25	0.92	5.6
VL-SAFE	552.43	69.17	4.25	146.7	132.55	0.7	0.05	0.34	0.46	5.22
Left Turn										
CLIPs	Return ↑	Cost ↓	AS ↑	WC ↑	TD ↑	AR ↑	CR ↓	TCF ↓	DCF ↓	CS ↓
VL-SAFE-NCNL	305.42	17.63	4.14	63	61.54	1	0	0	0	0
VL-SAFE-NC	281.87	0.22	5.12	70.9	61	1	0	0	0	0
VL-SAFE	422.96	0.21	3.19	72.8	60.77	1	0	0	0	0
Navigation										
CLIPs	Return ↑	Cost ↓	AS ↑	WC ↑	TD ↑	AR ↑	CR ↓	TCF ↓	DCF ↓	CS ↓
VL-SAFE-NCNL	528.86	48.41	7.08	297.55	321.43	0	0.1	0.39	0.36	3.04
VL-SAFE-NC	775.17	54.4	6.73	359	305.04	0	0.08	0.37	0.61	3.96
VL-SAFE	1074.96	9.15	4	253.2	184.6	0	0.04	0.08	0.19	1.18
Right Turn										
CLIPs	Return ↑	Cost ↓	AS ↑	WC ↑	TD ↑	AR ↑	CR ↓	TCF ↓	DCF ↓	CS ↓
VL-SAFE-NCNL	318.44	2.67	3.5	59.5	48.37	0.85	0	0	0	0
VL-SAFE-NC	258.61	0.72	4.49	60.9	48.01	0.93	0	0	0	0
VL-SAFE	315.17	0	2.53	58.1	43.5	0.89	0	0	0	0

lack semantic understanding of "safety" and often result in an over-conservative policy. In contrast, integrating VLM-based safety guidance effectively alleviates this issue by providing richer, semantic-level safety supervision.

#### F. Analysis on different types of CLIPs

We use CLIP [37] as our foundational safety estimator for each state in collected datasets. We tried four types of CLIPs under CarDreamer: (1) openai/clip-vit-base-patch32, (2) openai/clip-vit-large-patch14, (3) laion/CLIP-ViT-H-14-laion2B-s32B-b79K, and (4) laion/CLIP-ViT-bigG-14-laion2B-39B-b160k to identify which one provides superior results (we discuss the results in a subsequent section of this paper). The first CLIP model "openai/clip-vit-base-patch32" has a base-sized (151 million parameters) architecture. Similarly, "openai/clip-vit-large-patch14" has a larger size (428 million parameters). The model "laion/CLIP-ViT-H-14-laion2B-s32B-b79K" (986 million parameters) and "laion/CLIP-ViT-bigG-14-laion2B-39B-b160k" (2.5 billion parameters) are pre-trained on the LAION-2B dataset with 2.32 billion English image-text pairs [46]. They are dubbed as Base, Large, H, bigG, respectively. The experiment results are summarized in Table III.

In our analysis, we observed that the bigG model consistently outperformed all other models across all four tasks, showing the highest performance in terms of Return, Cost, and safety metrics such as AS, WC, TCF, DCF, and CS. This suggests that larger model parameters contribute to a more accurate understanding of the safety aspects in various driving scenarios. The substantial parameter size of bigG appears to enable a better grasp of the complex relationships involved in ensuring

vehicle safety, leading to more reliable performance, especially in challenging situations.

Moreover, it is important to note that the improvements in performance were not limited to a single metric such as Return. For safety-related metrics like Cost, CR, TCF, DCF, and CS, bigG showed significant improvements. This highlights that the increased model size not only enhances performance in terms of task completion but also makes the model more effective at minimizing risk and ensuring safety. Larger models, such as bigG, seem to offer a more robust assessment of safety, making them particularly beneficial in environments where the ability to detect and mitigate risks is critical.

In simpler tasks like Left Turn and Right Turn, the performance trend largely followed the expected pattern: larger models such as Large, H, and bigG tended to outperform the smaller Base model. This supports the idea that increasing model parameters improves the model's ability to handle less complex driving situations. Yet, when it came to more difficult tasks like Four Lane and Navigation, we observed that the larger models (H and Large) did not outperform the Base model. In some cases, their performance was even inferior to that of the smaller model, which suggests that simply increasing the model's size does not always lead to better results. This indicates that the benefits of larger models only become apparent when their parameter size exceeds a certain threshold, beyond which their performance improves, particularly in simpler scenarios.

#### G. Analysis on imagination capacities of world model

The experimental outcomes, as shown in Fig. 5, illustrate a comparison between ground-truth observations and predictions generated by the world model. Specifically, the top row

TABLE III  
ANALYSIS RESULTS ON DIFFERENT TYPES OF CLIPS

Four Lane										
CLIPs	Return ↑	Cost ↓	AS ↑	WC ↑	TD ↑	AR ↑	CR ↓	TCF ↓	DCF ↓	CS ↓
Base	521.11	106.74	3.87	144.2	129.41	0.4	0.09	0.32	0.86	3.86
Large	207.99	233.28	3.69	112.3	108.07	0.43	0.11	0.35	0.67	6.23
H	164.85	211.46	4.35	97	97	0.58	0.09	0.3	0.74	4.35
bigG	552.43	69.17	4.25	146.7	132.55	0.7	0.05	0.34	0.46	5.22
Left Turn										
CLIPs	Return ↑	Cost ↓	AS ↑	WC ↑	TD ↑	AR ↑	CR ↓	TCF ↓	DCF ↓	CS ↓
Base	358.7	1.68	2.18	71.5	60.63	0.94	0	0	0	0
Large	346.12	1.23	3.95	71	61.01	1	0	0	0	0
H	395.23	0.07	3.45	72.2	60.88	1	0	0	0	0
bigG	422.96	0.21	3.19	72.8	60.77	1	0	0	0	0
Navigation										
CLIPs	Return ↑	Cost ↓	AS ↑	WC ↑	TD ↑	AR ↑	CR ↓	TCF ↓	DCF ↓	CS ↓
Base	935.63	0.55	3.57	246.6	178.62	0	0.01	0.04	0.37	0
Large	411.34	60.93	7.12	343.5	301.11	0.01	0.06	0.36	0.24	5.88
H	718.72	76.44	4.72	262.5	235.67	0	0.07	0.17	0.42	2.65
bigG	1074.96	9.15	4	253.2	184.6	0	0.04	0.08	0.19	1.18
Right Turn										
CLIPs	Return ↑	Cost ↓	AS ↑	WC ↑	TD ↑	AR ↑	CR ↓	TCF ↓	DCF ↓	CS ↓
Base	153.72	0	0.43	26.5	20.95	0	0	0	0	0
Large	303.94	1.54	3.62	61.7	47.94	0.93	0	0	0	0
H	309.17	0	2.95	59.1	44.5	0.98	0	0	0	0
bigG	315.17	0	2.53	58.1	43.5	0.89	0	0	0	0

presents the actual observed frames, the middle row shows the predicted future frames by the world model, and the bottom row highlights the discrepancies between the two.

The results confirm the world model's capability to anticipate future scenes accurately across simulation platforms, the world model effectively forecasts vehicle motion, including straight paths and right turns, as well as the ego-relative rotation and translation of the BEV image.

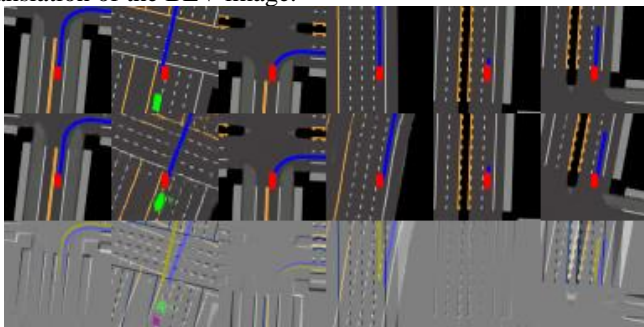


Fig. 5. Comparison between ground-truth observations and predictions generated by the world model.

## VII. CONCLUSIONS AND FUTURE WORK

This paper presents VL-SAFE, a novel framework designed to address multiple key limitations of RL-based autonomous driving, including low sample efficiency, poor generalization, etc. In particular, the proposed VLM-as-safety-guidance paradigm provides a semantic understanding of "safety" in complex driving contexts, enabling an effective safe policy learning. Specifically, we construct offline datasets collected by expert agents and labeled with safety scores derived from VLMs. A world model is trained to generate imagined rollouts

together with safety estimations, allowing the agent to perform safe planning without interacting with the real environment. Extensive experiments across multiple simulation platforms demonstrate that VL-SAFE achieves superior sample efficiency, generalization, safety, and overall performance compared to existing baselines.

One limitation of this study is that all experiments were conducted in a simulation environment. While simulation offers a controlled and reproducible setting, it cannot fully capture the complexities of the real world. A major contributor to this gap is the unrealistic behavior of background vehicles, which are typically controlled by rule-based models. These models fail to reflect the diverse and stochastic nature of human driving, leading to potential overfitting and poor generalization. A promising future direction is to develop a unified world model that learns more human-like background vehicle behaviors from real-world data, enabling more realistic simulations.

Another limitation lies in the use of pretrained VLMs for safety guidance. These models are trained on general datasets and may lack domain-specific understanding of driving scenarios. Fine-tuning VLMs for autonomous driving or exploring more advanced models like GPT-4o could improve semantic safety assessment and enhance policy robustness.

## APPENDIX

### A. Pseudo code of VL-SAFE

We demonstrate the pseudo code of our proposed method VL-SAFE here. There are two major parts corresponding to the overall framework in Fig. 3.

---

**Algorithm 1** VL-SAFE: Enhancing World Model-based Autonomous Driving with Safety-Guided Vision-Language Models
 

---

**Require:** Offline dataset  $\mathcal{D}$  with number of samples equal to  $S$ , policy  $\pi_\psi$ , critics  $Q_{\phi_1}$  and cost critics  $Q_{\phi_2}^c$ ,

- 1: value network  $V_{\phi_1}$  and cost value network  $V_{\phi_2}^c$ , VLM-guided world model  $p_\theta^{VLM}$ , the length of imaged rollouts  $H$ , the number of training steps  $N_{offline}$ .
- 2: Initialize model parameters  $\psi, \phi_k, \phi_k, \theta$ .
- 3: **for**  $i = 1, 2, \dots, S$  **do**
- 4:   Sample a batch of trajectory  $\mathcal{B}$  from  $\mathcal{D}_S$ .  
       Calculate VLM's safety estimation via  $p_t^{VLM} = \frac{Enc_I(I_t)^T Enc_T(T_t)}{\|Enc_I(I_t)\| \cdot \|Enc_T(T_t)\|}$
- 5:   Associate  $p_t^{VLM}$  with  $s_t$  in dataset  $\mathcal{D}$ .
- 7: **done**
- 8: **for**  $j = 1, 2, \dots, N_{offline}$  **do**
- 9:   Sample a batch of trajectory  $\mathcal{B}$  from  $\mathcal{D}_S$ .
- 10:   Compute model state  $s_t \sim p_\theta(s_t | s_{t-1})$ , where  $s_t \in \{h_t, z_t\}$ .  
       Update  $\theta$  using  $\mathcal{L}(\theta) \doteq E_{q_\theta} \sum_{t=1}^T (\beta_{pred} \mathcal{L}_{pred}^t(\theta) + \beta_{dyn} \mathcal{L}_{dyn}^t(\theta) + \beta_{rep} \mathcal{L}_{rep}^t(\theta))$
- 12:   Generate imagined rollouts with safety estimation using  $p_\theta^{VLM}$  for actor-critic learning
- 13:   Compute target estimation  $R_t$  via  $TD(\lambda)$
- 14:   Update  $V_{\phi_1}$  and  $V_{\phi_2}^c$  using  $\mathcal{L}_V(\phi)$
- 15:   Update  $Q_{\phi_1}$  and  $Q_{\phi_2}^c$  using  $\mathcal{L}_Q(\phi)$   
       Update  $\pi_\psi$  using  $\mathcal{L}_\pi(\psi)$ , where the policy updated is directed by  $w = p(s) \cdot \exp(\beta_1 A^r(s, \mathbf{a})) + (1 - p(s)) \cdot \exp(-\beta_2 A^c(s, \mathbf{a}))$ , and  $p(s)$  denotes the safety estimation for state  $s$ .
- 16:   Update  $\pi_\psi$  using  $\mathcal{L}_\pi(\psi)$ , where the policy updated is directed by  $w = p(s) \cdot \exp(\beta_1 A^r(s, \mathbf{a})) + (1 - p(s)) \cdot \exp(-\beta_2 A^c(s, \mathbf{a}))$ , and  $p(s)$  denotes the safety estimation for state  $s$ .
- 17: **done**

---

## B. Theoretical Interpolation

### B1. Theoretical Analysis of Stability of VLM-as-Safety-Guidance Paradigm

**Proposition 1.** The VLM-generated safety estimation is Lipschitz Continuous.

**Proof.** We show that the VLM-generated safety estimation is Lipschitz continuous with a provable upper bound. The original safety score is defined as:

$$p_t^{VLM} = \frac{Enc_I(I_t)^T Enc_T(T_t)}{\|Enc_I(I_t)\| \cdot \|Enc_T(T_t)\|} \quad (21)$$

The cosine similarity function is known to be 1 - Lipschitz under normalized inputs, and the sigmoid function  $\sigma(x)$  is 0.25-Lipschitz [47]. Therefore, the composition  $p_t^{VLM} = \sigma(\cos(\cdot))$  is at most 0.25-Lipschitz with respect to the latent feature  $Enc_I(I_t)$ . If the encoder itself is  $L_f$ -Lipschitz, then:

$$|p_1^{VLM} - p_2^{VLM}| \leq 0.25 \cdot \|Enc_I(I_1) - Enc_I(I_2)\| \leq 0.25 \cdot L_f \cdot \|I_1 - I_2\| \quad (22)$$

This establishes a theoretical upper bound on the Lipschitz constant of the safety estimation with respect to the state input, which is beneficial for stability in training and safety assurance in downstream planning.

**Remark 1.** Lipschitz continuity of the safety estimation function ensures that small changes in the input state lead to smooth and bounded changes in the safety estimate. This promotes stable training, improves generalization to unseen states, and enables reliable safety-aware planning and control. It also provides theoretical support for conservative exploration and robustness in imagined rollouts generated by world models.

### B2. Extraction of the optimal policy

The soft constraints from offline training can be solved by the proposition proposed by [49] as follows:

**Proposition 3.** Suppose that the optimizing problem has the following form:

$$\max_{\pi} \mathbb{E}_{a \sim \pi}[A(s, a)] \text{ s.t. } D_{KL}(\pi_\psi \parallel \pi_b) \leq \epsilon \quad (28)$$

The optimal solution will satisfy:

$$\pi^*(a | s) \propto \exp(\alpha A(s, a)) \pi_b(a | s) \quad (29)$$

**Proof.** The Lagrange function can be formulated as follows:

$$L(\pi_\psi, \lambda, \mu) = \mathbb{E}_{a \sim \pi}[A(s, a)] - \lambda(D_{KL}(\pi_\psi \parallel \pi_b) - \epsilon) \quad (30)$$

Then we take the partial derivative with respect to  $\pi$  and set it to 0:

$$\frac{\partial L}{\partial \pi_\psi} = A(s, a) - \lambda \log \pi_b(a | s) + \lambda \log \pi_\psi(a | s) = 0 \quad (31)$$

We have:

$$\pi^*(a | s) = \frac{1}{Z} \exp(\alpha A(s, a)) \pi_b(a | s) \quad (32)$$

where  $Z$  is a normalizing constant. Intuitively,  $\frac{1}{Z} \exp(\alpha A(s, a))$  is served as a weight  $w$  deciding the direction of policy updates towards maximizing the advantage function. Similarly, we can solve Eq. (15) by expressing the weight as:

$$w = p(s) \cdot \exp(\beta_1 A^r(s, \mathbf{a})) + (1 - p(s)) \cdot \exp(-\beta_2 A^c(s, \mathbf{a})) \quad (33)$$

### C. Hyper-parameters

World model has 512 GRU recurrent units, 32 CNN multipliers, 1024 dense hidden units, and 5 MLP layers. We use categorical distributions to represent the deterministic variable and stochastic variable in RSSM, providing more expressivity than using gaussian distributions as discussed in Dreamerv3 [9]. The cost limit is 0 and cost weight is 10, this is the same in [38]. The length of imaged rollouts is 16. The maximum simulation for one episode is 333 for CarDreamer, running out of road is considered a termination condition.

As discussed above, we apply weighted loss terms to balance the various learning objectives during the training of world models. The loss scales for different components are configured as follows: image reconstruction (1.0), vector reconstruction (1.0), reward (1.0), cost (1.0), continuation signal (1.0), dynamics consistency (0.5), representation learning (0.1), actor loss (1.0), critic loss (1.0), target network regularization (1.0), and safety prediction (1.0).

We adopt 350 k as the training steps for our proposed VL-SAFE Method (bigG as the default CLIP), even though keeping training can consistently reduce costs, but the policy will also become more conservative gradually with a lower average speed, and the episode might run out of time before the agent reaches to the destination. To achieve a balance between the costs and rewards, we choose 350 k as the training steps.

All online baseline methods are implemented and trained using Stable-Baselines3 [50], while offline methods are implemented using D3RLpy [51]. Unless otherwise specified, we adopt the default hyperparameter settings provided by these frameworks to ensure fair and reproducible comparisons. For algorithms that rely heavily on online interactions, such as SAC and DQN, we train each model for 1 million steps to ensure convergence and stable performance.

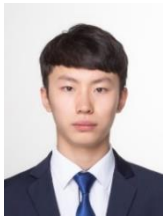
#### ACKNOWLEDGMENTS

This work was supported by Purdue University's branch of the Center for Connected and Automated Transportation (CCAT), a USDOT Region 5 University Transportation Center funded by US DOT Award #69A3552348305.

#### REFERENCES

- [1] K. Long, Z. Sheng, H. Shi, X. Li, S. Chen, and S. Ahn, "Physical enhanced residual learning (PERL) framework for vehicle trajectory prediction," *Commun. Transp. Res.*, vol. 5, p. 100166, 2025.
- [2] K. Long, Z. Liang, H. Shi, L. Shi, S. Chen, and X. Li, "Traffic oscillation mitigation with physics-enhanced residual learning (PERL)-based predictive control," *Commun. Transp. Res.*, vol. 4, p. 100154, 2024.
- [3] Y. Qu, Z. Li, X. Zhao, and J. Ou, "Towards real-world traffic prediction and data imputation: A multi-task pretraining and fine-tuning approach," *Inf. Sci.*, vol. 657, p. 119972, 2024.
- [4] Y. Qu, J. Rong, Z. Li, and K. Chen, "ST-A-PGCL: Spatiotemporal adaptive periodical graph contrastive learning for traffic prediction under real scenarios," *Knowl.-Based Syst.*, vol. 272, p. 110591, 2023.
- [5] Z. Sheng, Z. Huang, and S. Chen, "Kinematics-aware multigraph attention network with residual learning for heterogeneous trajectory prediction," *J. Intell. Connect. Veh.*, vol. 7, no. 2, pp. 138–150, 2024.
- [6] Y. Qu, Z. Huang, Z. Sheng, T. Chen, and S. Chen, "Towards 3D Semantic Scene Completion for Autonomous Driving: A Meta-Learning Framework Empowered by Deformable Large-Kernel Attention and Mamba Model," *ArXiv Prepr. ArXiv241103672*, 2024.
- [7] S. Zhang, W. Huang, Z. Gao, H. Chen, and C. Lv, "WiseAD: Knowledge Augmented End-to-End Autonomous Driving with Vision-Language Model," *ArXiv Prepr. ArXiv241209951*, 2024.
- [8] Z. Huang, Z. Sheng, C. Ma, and S. Chen, "Human as AI mentor: Enhanced human-in-the-loop reinforcement learning for safe and efficient autonomous driving," *Commun. Transp. Res.*, vol. 4, p. 100127, 2024.
- [9] D. Hafner, J. Pasukonis, J. Ba, and T. Lillicrap, "Mastering diverse domains through world models," *ArXiv Prepr. ArXiv230104104*, 2023.
- [10] D. Hafner, T. Lillicrap, M. Norouzi, and J. Ba, "Mastering atari with discrete world models," *ArXiv Prepr. ArXiv201002193*, 2020.
- [11] D. Hafner, T. Lillicrap, J. Ba, and M. Norouzi, "Dream to control: Learning behaviors by latent imagination," *ArXiv Prepr. ArXiv191201603*, 2019.
- [12] K. Qian *et al.*, "FASIONAD++: Integrating High-Level Instruction and Information Bottleneck in FAT-Slow fusION Systems for Enhanced Safety in Autonomous Driving with Adaptive Feedback," *ArXiv Prepr. ArXiv250308162*, 2025.
- [13] Z. Sheng, Z. Huang, and S. Chen, "Traffic expertise meets residual RL: Knowledge-informed model-based residual reinforcement learning for CAV trajectory control," *Commun. Transp. Res.*, vol. 4, p. 100142, 2024.
- [14] J. Wu, Y. Zhou, H. Yang, Z. Huang, and C. Lv, "Human-guided reinforcement learning with sim-to-real transfer for autonomous navigation," *IEEE Trans. Pattern Anal. Mach. Intell.*, vol. 45, no. 12, pp. 14745–14759, 2023.
- [15] S. Levine, A. Kumar, G. Tucker, and J. Fu, "Offline reinforcement learning: Tutorial, review, and perspectives on open problems," *ArXiv Prepr. ArXiv200501643*, 2020.
- [16] P. Koirala, Z. Jiang, S. Sarkar, and C. Fleming, "Latent Safety-Constrained Policy Approach for Safe Offline Reinforcement Learning," *ArXiv Prepr. ArXiv241208794*, 2024.
- [17] I. Kostrikov, A. Nair, and S. Levine, "Offline reinforcement learning with implicit q-learning," *ArXiv Prepr. ArXiv211006169*, 2021.
- [18] A. Kumar, A. Zhou, G. Tucker, and S. Levine, "Conservative q-learning for offline reinforcement learning," *Adv. Neural Inf. Process. Syst.*, vol. 33, pp. 1179–1191, 2020.
- [19] M. Rigter, B. Lacerda, and N. Hawes, "Rambo-rl: Robust adversarial model-based offline reinforcement learning," *Adv. Neural Inf. Process. Syst.*, vol. 35, pp. 16082–16097, 2022.
- [20] Q. Li, X. Jia, S. Wang, and J. Yan, "Think2Drive: Efficient Reinforcement Learning by Thinking with Latent World Model for Autonomous Driving (in CARLA-V2)," presented at the European Conference on Computer Vision, Springer, 2024, pp. 142–158.
- [21] Y. Wang, J. He, L. Fan, H. Li, Y. Chen, and Z. Zhang, "Driving into the future: Multiview visual forecasting and planning with world model for autonomous driving," presented at the Proceedings of the IEEE/CVF Conference on Computer Vision and Pattern Recognition, 2024, pp. 14749–14759.
- [22] X. Wang, Z. Zhu, G. Huang, X. Chen, J. Zhu, and J. Lu, "DriveDreamer: Towards Real-World-Drive World Models for Autonomous Driving," presented at the European Conference on Computer Vision, Springer, 2024, pp. 55–72.
- [23] X. Hu, P. Chen, Y. Wen, B. Tang, and L. Chen, "Long and Short-Term Constraints Driven Safe Reinforcement Learning for Autonomous Driving," *ArXiv Prepr. ArXiv240318209*, 2024.
- [24] W. Huang, H. Liu, Z. Huang, and C. Lv, "Safety-aware human-in-the-loop reinforcement learning with shared control for autonomous driving," *IEEE Trans. Intell. Transp. Syst.*, 2024.
- [25] J. Zhou, L. Yan, and K. Yang, "Enhancing system-level safety in mixed-autonomy platoon via safe reinforcement learning," *IEEE Trans. Intell. Veh.*, 2024.
- [26] H. Pan, M. Luo, J. Wang, T. Huang, and W. Sun, "A safe motion planning and reliable control framework for autonomous vehicles," *IEEE Trans. Intell. Veh.*, vol. 9, no. 4, pp. 4780–4793, 2024.
- [27] J. Li, D. Li, S. Savarese, and S. Hoi, "Blip-2: Bootstrapping language-image pre-training with frozen image encoders and large language models," presented at the International conference on machine learning, PMLR, 2023, pp. 19730–19742.
- [28] J. Li, D. Li, C. Xiong, and S. Hoi, "Blip: Bootstrapping language-image pre-training for unified vision-language understanding and generation," presented at the International conference on machine learning, PMLR, 2022, pp. 12888–12900.
- [29] H. Lu *et al.*, "Deepseek-vl: towards real-world vision-language understanding," *ArXiv Prepr. ArXiv240305525*, 2024.
- [30] P. Wang *et al.*, "Qwen2-vl: Enhancing vision-language model's perception of the world at any resolution," *ArXiv Prepr. ArXiv240912191*, 2024.
- [31] M. J. Kim *et al.*, "Openvla: An open-source vision-language-action model," *ArXiv Prepr. ArXiv240609246*, 2024.
- [32] X. Tian *et al.*, "Drivevlm: The convergence of autonomous driving and large vision-language models," *ArXiv Prepr. ArXiv240212289*, 2024.
- [33] Y. Xu *et al.*, "Vlm-ad: End-to-end autonomous driving through vision-language model supervision," *ArXiv Prepr. ArXiv241214446*, 2024.
- [34] Z. Sheng, Z. Huang, Y. Qu, Y. Leng, S. Bhavanam, and S. Chen, "CurricuVLM: Towards Safe Autonomous Driving via Personalized Safety-Critical Curriculum Learning with Vision-Language Models," *ArXiv Prepr. ArXiv250215119*, 2025.
- [35] Z. Huang, Z. Sheng, Y. Qu, J. You, and S. Chen, "VLM-RL: A Unified Vision Language Models and Reinforcement Learning Framework for Safe Autonomous Driving," *ArXiv Prepr. ArXiv241215544*, 2024.
- [36] X. Ye, F. Tao, A. Mallik, B. Yaman, and L. Ren, "Lord: Large models based opposite reward design for autonomous driving," *ArXiv Prepr. ArXiv240318965*, 2024.
- [37] A. Radford *et al.*, "Learning transferable visual models from natural language supervision," presented at the International conference on machine learning, PMLR, 2021, pp. 8748–8763.
- [38] C. Cao *et al.*, "FOSP: Fine-tuning Offline Safe Policy through World Models," *ArXiv Prepr. ArXiv240704942*, 2024.
- [39] M. Ganai, Z. Gong, C. Yu, S. Herbert, and S. Gao, "Iterative reachability estimation for safe reinforcement learning," *Adv. Neural Inf. Process. Syst.*, vol. 36, pp. 69764–69797, 2023.

- [40] X. B. Peng, A. Kumar, G. Zhang, and S. Levine, "Advantage-weighted regression: Simple and scalable off-policy reinforcement learning," *ArXiv Prepr. ArXiv191000177*, 2019.
- [41] D. Gao, S. Cai, H. Zhou, H. Wang, I. Soltani, and J. Zhang, "Cardreamer: Open-source learning platform for world model based autonomous driving," *IEEE Internet Things J.*, 2024.
- [42] A. Dosovitskiy, G. Ros, F. Codevilla, A. Lopez, and V. Koltun, "CARLA: An open urban driving simulator," presented at the Conference on robot learning, PMLR, 2017, pp. 1–16.
- [43] J. Schulman, F. Wolski, P. Dhariwal, A. Radford, and O. Klimov, "Proximal policy optimization algorithms," *ArXiv Prepr. ArXiv170706347*, 2017.
- [44] T. Haarnoja, A. Zhou, P. Abbeel, and S. Levine, "Soft actor-critic: Off-policy maximum entropy deep reinforcement learning with a stochastic actor," presented at the International conference on machine learning, Pmlr, 2018, pp. 1861–1870.
- [45] V. Mnih *et al.*, "Playing atari with deep reinforcement learning," *ArXiv Prepr. ArXiv13125602*, 2013.
- [46] C. Schuhmann *et al.*, "Laion-5b: An open large-scale dataset for training next generation image-text models," *Adv. Neural Inf. Process. Syst.*, vol. 35, pp. 25278–25294, 2022.
- [47] X. Qi, J. Wang, Y. Chen, Y. Shi, and L. Zhang, "Lipsformer: Introducing lipschitz continuity to vision transformers," *ArXiv Prepr. ArXiv230409856*, 2023.
- [48] S. G. Bobkov and F. Götze, "Exponential integrability and transportation cost related to logarithmic Sobolev inequalities," *J. Funct. Anal.*, vol. 163, no. 1, pp. 1–28, 1999.
- [49] A. Nair, A. Gupta, M. Dalal, and S. Levine, "Awac: Accelerating online reinforcement learning with offline datasets," *ArXiv Prepr. ArXiv200609359*, 2020.
- [50] A. Raffin, A. Hill, A. Gleave, A. Kanervisto, M. Ernestus, and N. Dormann, "Stable-baselines3: Reliable reinforcement learning implementations," *J. Mach. Learn. Res.*, vol. 22, no. 268, pp. 1–8, 2021.
- [51] T. Seno and M. Imai, "d3rlpy: An offline deep reinforcement learning library," *J. Mach. Learn. Res.*, vol. 23, no. 315, pp. 1–20, 2022.



**Yansong Qu** was born in Dalian, Liaoning, China, in 1999. He received his Bachelor's degree in Traffic Engineering from Dalian Jiaotong University, Dalian, China, in 2021, and his Master's degree from the College of Metropolitan Transportation at Beijing University of Technology, Beijing, China. He is currently pursuing his Ph.D. in Civil Engineering at Purdue University. His research interests include autonomous driving simulation, reinforcement learning, and vision-language models.



**Zilin Huang** received the B.S. degree in mechanical engineering from the School of Electromechanical Engineering, Guangdong University of Technology in 2018. He received the M.S. degree in Communication and Transportation Engineering from South China University of Technology in 2021. He is currently pursuing the Ph.D. degree at the Department of Civil and Environmental Engineering, University of Wisconsin-Madison, USA. Before joining UW-

Madison, he worked at the Center for Connected and Automated Transportation (CCAT), Purdue University, USA. His research interests include human-centered AI, autonomous driving, robotics, human-robot interaction, and intelligent transportation.



**Zihao Sheng** received his B.S. degree in Automation from Xi'an Jiaotong University, Xi'an, China in 2019 and M.S. degree in Control Engineering from Shanghai Jiao Tong University, Shanghai, China in 2022. He is currently pursuing a Ph.D. degree at the Department of Civil and Environmental Engineering, University of Wisconsin-Madison, USA. His main research interests include human-centered AI, autonomous driving, reinforcement learning, and intelligent transportation.



in autonomous driving systems.

**Jiancong Chen** received his B.S. degree in Transportation and Communication from Chang'an University, Xi'an, China in 2021 and M.S. degree in Transportation Engineering from Southeast University, Nanjing, China in 2024. He is currently pursuing a Ph.D. degree at the Lyles School of Civil and Construction Engineering, Purdue University, USA. His research interests lie at the intersection of Artificial Intelligence, Statistics and Robotics, with a focus on their integration



**Sikai (Sky) Chen** is an Assistant Professor at the Department of Civil and Environmental Engineering and the Department of Mechanical Engineering (courtesy), University of Wisconsin-Madison. He received his Ph.D. in Civil Engineering with a focus on Computational Science & Engineering from Purdue University in 2019. His research centers around three major themes: human users, AI, and transportation. He aims to innovate and develop safe, efficient, sustainable,

and human-centered transportation systems using cutting-edge methods and technologies. The focus is on incorporating human behaviors, interactive autonomy, digital infrastructure, and intelligent control frameworks. In addition, he is a member of two ASCE national committees: Connected & Autonomous Vehicle Impacts, and Economics & Finance; IEEE Emerging Transportation Technology Testing Technical Committee, and TRB Standing Committee on Statistical Methods (AED60).



**Samuel Labi** is a professor at Purdue University, associate director of the USDOT Center for Connected & Automated Transportation, and Director of the Midwest branch of FHWA's Center of Excellence in Project Finance. He has authored 2 course-instruction textbooks: Transportation Decision Making (2008) and Civil Engineering Systems (2014) and serves in editorial roles for journals including Computer-Aided Civil & Infrastructure Engineering and the Journal of Intelligent & Connected Vehicles. Dr. Labi chairs the Planning & Development Council of the American Society of Civil Engineers' Transportation & Development Institute. His research awards include the American Society of Tests and Materials (ASTM)'s Mather Award (2007); TRB's K.B. Woods (2008) and Grant Mickle (2019) awards; and ASCE's Frank Masters (2014) and Wilbur Smith (2025) awards.